Talanta 260 (2023) 124586

Contents lists available at ScienceDirect

Talanta

journal homepage: www.elsevier.com/locate/talanta

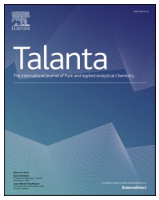

Label-free electrochemical immunosensor for Ochratoxin a detection in coffee samples

Jairo Pinto de Oliveira [a,b,*], Francisco Burgos-Flórez [a,c], Isabella Sampaio [a], Pedro Villalba [d], Valtencir Zucolotto [a]

[a] Nanomedicine and Nanotoxicology Group, São Carlos Institute of Physics, University of São Paulo, CP 369, 13560-970, São Carlos, SP, Brazil
[b] Federal University of Espírito Santo, Av Marechal Campos 1468, Vitória, ES 29.040-090, Brazil
[c] Health and Technological Innovation, Universidad Simón Bolívar, Facultad de Ingenierías, Barranquilla, 080002, Colombia
[d] Department of Medicine, Health Division, Universidad Del Norte, Barranquilla, 081007, Colombia

ARTICLE INFO

Handling Editor: J.M. Kauffmann

Keywords:
Ochratoxin A
Immunosensor
Label-free
Coffee
Electrochemical biosensor

ABSTRACT

Ochratoxin A (OTA) is a nephrotoxic and carcinogenic mycotoxin frequently found in coffee, which directly impacts human health and the economy of many countries. For this reason, there has been a growing need for simple and sensitive tools for the on-site detection of this mycotoxin. In this study, we developed a label-free impedimetric immunosensor to detect OTA. The biosensor was built on a thin-film gold electrode evaporated on glass substrtes, modified with a self-assembled cysteamine monolayer and anti-OTA antibodies. Atomic force microscopy and Microspectroscopy RAMAN confirmed the successful functionalization of the electrodes. The biosensor performance was evaluated by electrochemical impedance spectroscopy and the measurements indicated a linear relationship between the change in the impedance values and the OTA concentration in the range from 0.5 to 100 ng mL^{-1} with a limit of detection of 0.15 ng mL^{-1}. The biosensor was highly selective and did not suffer matrix interference when analyzed in coffee samples. Furthermore, considering the small sample volumes, the short time required for analysis, and the possibility of miniaturization, the developed biosensor represents a promising analytical device for on-site coffee quality analyses.

1. Introduction

According to the World Health Organization (WHO), mycotoxins endanger human health, animal production, and the economy of many countries [1]. Special attention has been given to the presence of Ochratoxin A (OTA) in coffee beans, one of the most valuable commodities in world trade, second only to oil as a source of income for developing countries [2]. OTA is produced by fungi of various *Aspergillus* and *Penicillium* species that grow in crops, or during storage. This toxin is highly resistant to a wide range of environmental conditions, withstanding high acidity levels and temperatures, which makes its elimination difficult [3]. Treatment of OTA in coffee beans is also limited by the detection methods available, which are hindered by the matrix [4,5].

In recent years, research on the harm to human or animal health caused by OTA has become a high-profile topic. This mycotoxin is nephrotoxic and carcinogenic and appears to compete with natural phenylalanine in protein synthesis involving phenylalanine-tRNA synthetase. OTA has also been reported to affect the inhibition/activation of enzymes during protein synthesis and apoptosis [6,7], immunosuppression [8], alteration in immune cell activities [9], endocrine disruption [10], and modulation of cytokine production [11].

Currently, the analysis of OTA in grains and foods is performed by high-performance liquid chromatography, generally associated with mass spectrometry. In addition, ELISA immunoassays (such as direct, indirect, competitive, and sandwich) are widely used and recognized as excellent and accurate for mycotoxin screening. However, these techniques have complex operations, require highly qualified personnel, and need long analysis time. For these reasons, simple detection methods for on-site detection are in great demand.

In this regard, strategies using optical transducers [12–14] and electrochemical sensors [15–19] have considerably expanded the range of possibilities for mycotoxin detection. Electrochemical systems, in particular, are promising for this purpose because they present high sensitivity, miniaturization feasibility, low cost, and do not suffer interference from matrix staining in complex samples. Recently, Wang

* Corresponding author. Federal University of Espírito Santo, Av Marechal Campos 1468, Vitória, ES Brazil.
E-mail address: jairo.oliveira@ufes.br (J.P. de Oliveira).

https://doi.org/10.1016/j.talanta.2023.124586
Received 19 December 2022; Received in revised form 17 April 2023; Accepted 21 April 2023
Available online 22 April 2023

et al. (2019) [20] reported excellent results using an electrochemical aptasensor with signal amplification through an exonuclease with a linear OTA detection range from 10 pg mL^{-1} to 10 ng mL^{-1} and LOD of 3 pg mL^{-1}. Liu et al. [21] developed a competitive electrochemical immunosensor in which the electrochemical response resulting from the oxidation of the enzyme product was inversely proportional to the OTA concentration in the range of 10 pg mL^{-1} to 100 ng mL^{-1}, with a limit of detection (LOD) as low as 8.2 pg mL^{-1}.

To date, few studies have reported the use of label-free impedimetric immunosensors for OTA detection. These systems have made tremendous progress in recent years due to their ability to quickly detect the mycotoxin in small reaction volumes [22]. Malvano et al. developed a biosensor for measuring OTA in cocoa beans, with a linear detection range from 0.01 to 5 ng mL^{-1} and a LOD of 0.01 ng mL^{-1} [23]. Muchindu et al. reported a system for OTA detection in a linear range from 2 to 10 ng mL^{-1} and a LOD of 10 $pg.kg^{-1}$using passive immobilization of anti-OTA antibodies on a platinum electrode modified with sulfonated polyaniline [24]. Radi et al. constructed a polycrystalline gold electrode with 4-carboxyphenyl film grafted by electrochemical reduction [25]. This impedimetric immunosensor had a linear detection range of 1–20 ng mL^{-1} and a LOD of 0.5 ng mL^{-1}. Kunene et al. developed an electrochemical aptasensor for OTA detection in cereal by immobilizing an OTA aptamer and bovine serum albumin on carbon screen printed electrodes modified with silver nanoparticles and reduced graphene oxide, obtaining a linear range from 0.002 to 0.016 mg L^{-1} and a LOD of 7×10^{-4} mg L^{-1} [26]. Despite advances in enhancing the detection limits, the strategies reported did not address selectivity and were based on complex methods involving multiple steps for fabricating the biosensors.

In this study, an immunosensor based on electrochemical impedance spectroscopy (EIS) was optimized for label-free detection of OTA in coffee beans samples. The electrodes were built on BK7 glass substrates covered with 105 nm-thick gold tracks. Cysteamine was used as a thiol ligand for forming self-assembled monolayers (SAMs), and anti-OTA antibodies were immobilized by Carboxyl activation on the constant region of the antibody. Experimental parameters regarding electrodes cleaning, antibody concentration, and incubation times were evaluated to improve the immunosensors performance. As a result, the developed system detected OTA within limits applicable to international legislation and proved reproducible, selective, and applicable to real samples.

2. Materials and methods

2.1. Materials

Ochratoxin A (CAS 303-47-9, >98%, Sigma Aldrich, 01877), Ochratoxin B (CAS 4825-86-9, >97%, Sigma Aldrich, 32411) were purchased from Sigma Aldrich. Rabbit polyclonal Anti-Ochratoxin A antibody was acquired from Abcam (NR, >98%, Abcam, 35133). N-(3-Dimethylaminopropyl)-N′-ethylcarbodiimide hydrochloride (CAS 25952-53-8, >98%, Sigma Aldrich, 03450), N-Hydroxysuccinimide (CAS 6066-82-6, >97%, Sigma Aldrich, 56480), Potassium ferricyanide (III) (CAS 13746-66-2, >99%, Sigma Aldrich, 702587), Potassium chloride (CAS 7447-40-7, >99%, Sigma Aldrich, P4504), Cysteamine (CAS 60-23-1, >98%, Sigma Aldrich, 30070), Sodium phosphate monobasic dihydrate (CAS 13472-35-0, >99%, Sigma Aldrich, 71500), Sodium phosphate dibasic (CAS 7558-79-4, >99%, Sigma Aldrich, S5136), Bovine Serum Albumin (CAS 9048-46-8, >98%, Sigma Aldrich, A7906) were purchased from Sigma Aldrich and used without further purification. Acetone (CAS 67-64-1, >99.9%, Synth), Ethanol (CAS 64-17-5, >99.9%, Synth), Potassium permanganate (CAS 7722-64-7, >99.5%, Synth), Hydrogen peroxide (CAS 7722-84-1, 35%, Synth) and Potassium hydroxide (CAS 1310-58-3, >99.9%, Synth) were acquired from Synth. Ultrapure Water 18.2 MΩ cm resistivity was obtained using a Mega Purity system.

2.2. Electrodes fabrication

Disposable devices comprising a reference electrode, a counter electrode and a working electrode (7 mm^2 of geometric area) were fabricated in the Brazilian Nanotechnology National Laboratory (LNNano) of the National Center for Research in Energy and Material (CNPEM), Brasil. The electrodes pattern was impressed on glass substrates by photolithography and the metallization of the adhesion layer (chromium, 15 nm) and the gold surface layer (105 nm) was performed by sputtering technique with a quartz crystal to measure their thickness. Electrodes were cleaned in oxygen plasma to remove organic residues (Tergeo Plasma Cleaner, Pie Scientific). Alternatively, a strategy using chemical cleaning was also evaluated in four steps using acetone, water, 2% potassium hydroxide in ethanol, and pure ethanol. During washing, the electrodes were immersed in each cleaning solution and submitted to ultrasound for 15 min.

Surface modification of the working electrodes was performed by the SAM technique. For this, 3 μL of 0.5 M cysteamine solution was added to the electrode and left for 12 h, to form a monolayer with free NH2. After gentle washing with ultrapure water, 3 μL of a solution containing the antibodies was added to the electrode allowing the antibodies to immobilize on the surface through covalent binding mediated by the EDC-NHS system. The antibodies were previously activated with 8 mM EDC and 5 mM NHS in 10 mM PBS (pH 7.2) for 2 h. The incubation time and concentration of the antibodies in the working electrode was evaluated according to the experimental design. Following, 1% Glycine in 10 mM PBS (pH 7.2) was added to the electrode's surface for 30 min, aiming at blocking the nonspecific binding sites. For detection assays, 3 μL of samples containing different toxin concentrations were incubated for 30 min on the working electrodes. Before the electrochemical measurements, the electrodes were gently washed with PBS and ultrapure water.

2.3. Optimization tests

The cleaning steps in oxygen plasma, concentration of the antibodies, and the incubation time for immobilization of the antibodies were subjected to optimization. Table 1 presents the parameters and their tested variations. All experiments were performed in triplicate.

2.4. Characterization of the electrodes

The electrodes were characterized by energy dispersive x-rays (EDS) using a Bruker XFlash 6/10 detector coupled to a scanning electron microscope (SEM) model JEM 6610 LV (JEOL, USA) operated at 20 kV with a tungsten filament. The formation of a cysteamine SAM and the antibody immobilization on the electrodes were confirmed using Raman spectroscopy with a 532 nm laser and spectral resolution of 0.3 cm^{-1} (Renishaw, Invia Raman microscope). In addition, atomic force microscopy (NanoSurf Flexa) was used to determine changes in the average surface roughness of the electrodes before and after immobilization.

2.5. Electrochemical measurements

Electrochemical measurements were performed using 0.1 M KCl as the supporting electrolyte and 5 mM potassium ferrocyanide as the

Table 1
Optimized parameters for the construction of the impedimetric immunosensor for OTA detection.

Parameter	Variations
Electrode cleaning protocol	Chemical/Plasma Oxygen
Plasma time (s)	30/60/90
Antibody concentration (ug.mL^{-1})	10/25/50/100/200
Antibody incubation time (h)	0.5/2/4/12

redox probe. EIS analyses were performed in an Autolab potentiostat (Metrohm) with 10 mV rms at zero volts of DC bias, with frequencies between 10 KHz and 0.1 Hz The frequency range was from 10 kHz to 0.1 Hz. Nyquist plots and charge transfer resistance (R_{CT}) were obtained using the NOVA 2.1 software.

2.6. Data analyses

Origin Pro 8.5 free version and GraphPad Prism version 6.01 were used for Nyquist and Raman spectra plots and statistical analysis. The free software Gwyddion version 2.61 was used to process the AFM data. Finally, ChemDraw Prime software (courtesy of PerkinElmer) was used to create schematics.

3. Results and discussion

3.1. Electrodes characterization

The electrode's surface was characterized by AFM in all stages of immunosensor fabrication (Fig. 1A and B). The images reveal an increase in roughness after the formation of SAMs with cysteamine, and after the immobilization of the antibodies by covalent coupling. The roughness profile shows the maximum distance between the deepest valley and the highest peak for the three electrodes evaluated: 6.2 nm for the clean electrode, 9.3 nm for the electrode with the cysteamine SAM, and 13.6 nm for the electrode with immobilized antibodies (Fig. 1A and B). The SEM and EDS characterization of electrodes are shown in Fig. S1 (Supplementary Material).

The treatment of the electrode surface with oxygen plasma, cysteamine SAM formation, and the antibody immobilization step were also confirmed by Raman spectroscopy (Fig. 1C). The band intensities across the spectrum are reduced after plasma treatment, indicating that this technique is efficient for removing organic matter, allowing a high level of chemical functionalization on the surface of the electrodes. A discrete band visible at 1385 cm^{-1} is typically associated with amorphous carbon [27]. After incubation with cysteamine, a well-defined band at 856 cm^{-1} is observed, corresponding to the free NH groups and CH_2 rocking, and a band at 1090 cm^{-1}, attributed to SC vibrations, indicating the successful immobilization of these molecules [28,29]. On the electrode with immobilized antibodies, a low-intensity band at 543 cm^{-1} characteristics of disulfide bonds (S–S) can be seen [30]. This covalent bonding occurs between the SH of the ligand and the SH of cysteine and methionine residues in the antibody structure. The band at 849 cm^{-1} is attributed to vibrations of NH groups [28]. The Raman shift to a lower wavenumber means that the vibrational frequency of the molecule is lowered, which can be taken as evidence of chemical bond elongation due to tensile stress.

3.2. Optimization of the electrochemical immunosensor

Electrodes cleaning

To evaluate the influence of plasma time on contaminant removal, the electrodes were characterized by EIS after the cleaning procedure. Nyquist plots show the relationship between the real and imaginary impedance components for a range of frequencies and are commonly used to evaluate the resistive component of the system. The semicircle in high-frequency regions describes the electron transfer process. In contrast, the low-frequency linear region contains information about the mass transport of redox species at the electrolyte-electrode interface. Impedance data were fitted to the Randles model to determine R_{CT} values, which were significantly reduced with plasma oxygen treatment comparing with the chemical cleaning (Fig. 2A).

Oxygen plasma is a practical, economical, and environmentally safe method for cleaning electrodes. The generated vacuum UV energy effectively breaks most of the organic bonds of surface contaminants [31]. In addition, oxygen species created in the plasma react with

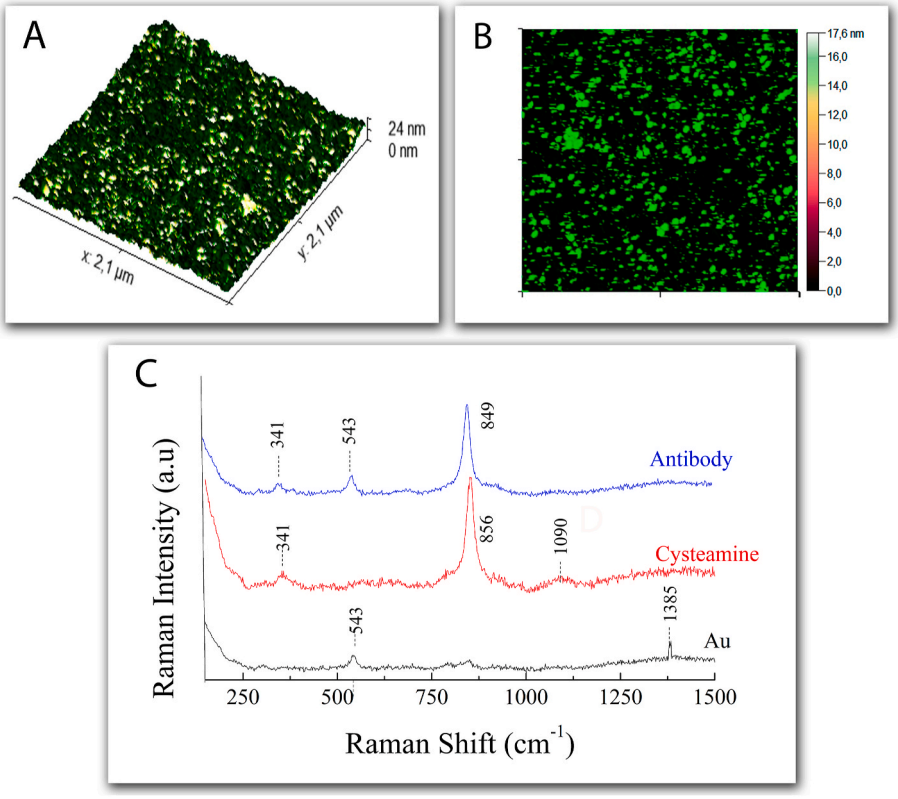

Fig. 1. Topography images obtained by atomic force microscopy in 3D (A) and in 2D (B).Raman spectra from clean electrodes, functionalized with cysteamine, and immobilized antibodies (C).

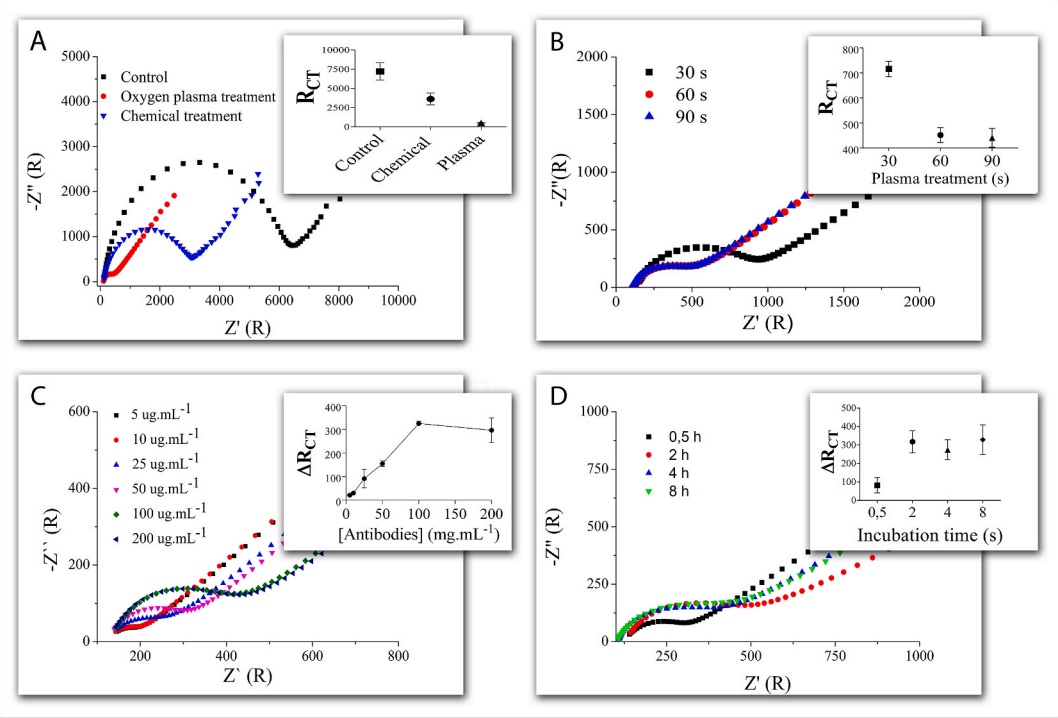

Fig. 2. Nyquist plots of the biosensor relative to chemical and physical cleaning (A); Treatment with oxygen plasma at different times (B); concentrations (C) and time (D) for covalent coupling of immobilized antibodies. The insets show the variations in R_{CT} values. Delta R_{CT} values correspond to the difference between the RCT before and after antibody immobilization.

organic contaminants and are evacuated from the chamber during processing. The resulting surface is ultra clean [32]. The plasma treatment times were evaluated (Fig. 2B), and there was a significant reduction in R_{CT} values from 30 to 60 s. Since the cleaning time of 90 s did not change the R_{CT} values, a 60-s time was chosen for the subsequent experiments.

Antibody concentration

The amount of immobilized antibodies and their orientation play a critical role in the biosensor performance. Therefore, the amount of antibodies needed to cover the entire surface of the working electrode was determined using the covalent coupling method with the EDC/NHS system. For this, EIS spectra were collected and the data presented in the Nyquist diagram (Fig. 2C). The change in R_{CT} values may reflect the amount of immobilized antibodies. In addition, an increase in the formed organic layer makes the diffusion of electrons towards the surface of the electrode more difficult and, consequently, increases the R_{CT} values. Based on the R_{CT} values observed, one can notice that saturation occurs at 100 μg mL^{-1}, indicating that this concentration was sufficient to cover the entire available area of the working electrode.

Antibody incubation time

The incubation time required for antibody immobilization on the electrodes was investigated using EIS. In general terms, for covalent immobilization strategies, the longer the time, the greater the possibility of reaching the equilibrium point of the coupling reaction. However, long times can promote solvent evaporation, sample dehydration, non-homogeneous distribution, and aggregation [33], with direct impacts the sensitivity and reproducibility of a biosensor. Nevertheless, as can be seen in the Nyquist plots (Fig. 2C), the time of 2 h was enough to stabilize the variations in the R_{CT} values.

3.3. Fabrication of the immunosensor

After optimizing the parameters to improve the immunosensor performance, EIS was used to characterize each step for assembling the impedimetric sensors (Fig. 3). The Nyquist diagram of the four biosensor steps included: 1) cleaning the electrode with oxygen plasma; 2) forming the cysteamine SAM; 3) immobilization of anti-OTA antibodies; 4) glycine blocking.

The clean electrodes exhibited a low resistance to electron transfer from the redox probe (R_{CT} = 417 Ω). The formation of the monolayer with thiol ligand decreased the R_{CT} value to 86 Ω. This coating provides a stable surface to immobilize the bioreceptors and creates a dielectric between the surface and the medium. The decrease in the R_{CT} value is related to the positive charge mediated by free NH_2 groups on the surface, which favors electrons diffusion. Subsequently, anti-OTA antibodies previously activated by EDC-NHS were immobilized on the electrode surface (R_{CT} = 335 Ω). The increase in R_{CT} at this stage can be attributed to the bulk properties of the antibody molecules, which introduce an insulating barrier at the electrode/electrolyte interface. The remarkable increase in R_{CT} value compared to the previous step favor a wider dynamic range for OTA detection assays. A subtle increase in R_{CT} values (R_{CT} = 433 Ω) after blocking the electrodes with glycine was also observed, probably due to the small size of this molecule.

3.4. Electrochemical detection of OTA

For OTA detection assays, concentrations from 0.1 to 200 ng mL^{-1} of OTA were evaluated by EIS, and R_{CT} values were determined (Fig. 4). We observed a proportional increment of R_{CT} values as OTA concentration was increased. The binding of OTA to antibodies can provide an additional negative charge due to the presence of ionizable carboxylic acids and hydroxyls in the chemical structure of the mycotoxin. It has been discussed that conformational changes of the antibody molecules after the formation of the complex with the antigen may hinder the transfer of electrons and, consequently, increase R_{CT} values [25]. A linear relationship was observed between 0.5 and 100 ng mL^{-1} OTA concentrations, while saturation occurred at 200 ng mL^{-1}, probably due to steric hindrance or saturation of coupled OTA molecules [34]. The

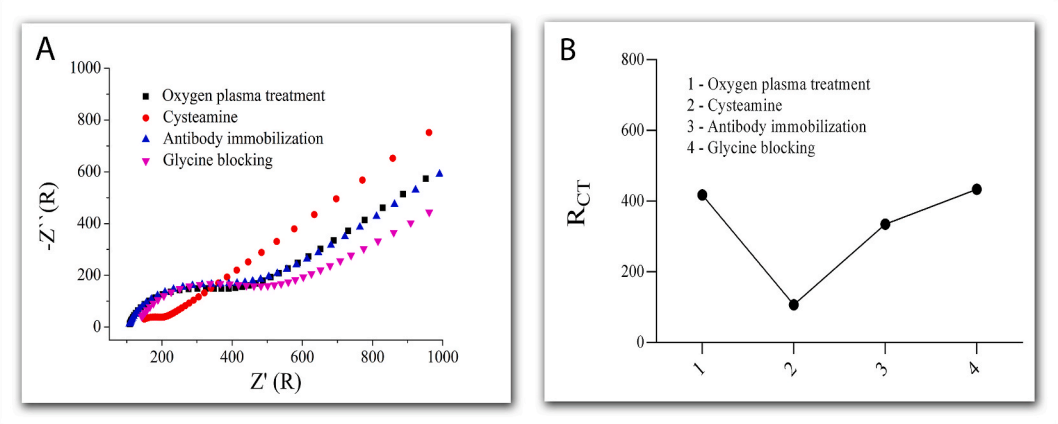

Fig. 3. Nyquist plots of immunosensor fabrication steps (A). Variations in R_{CT} values as a function of immunosensor construction steps (B).

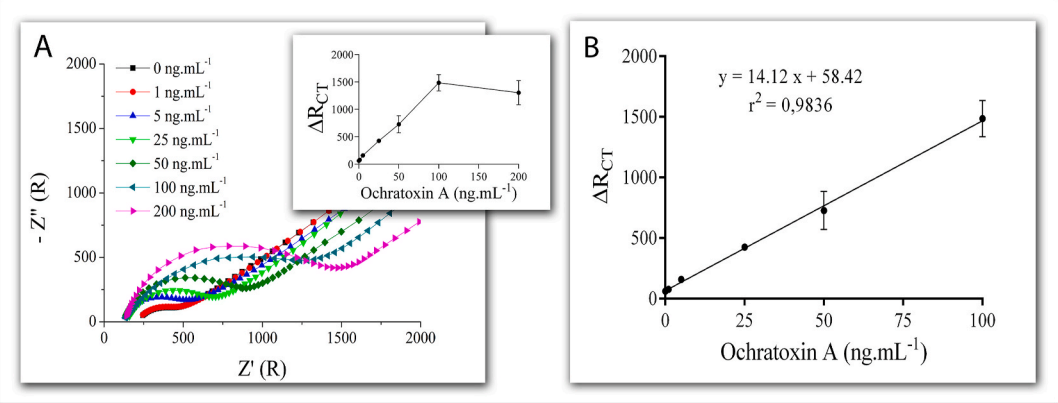

Fig. 4. Nyquist plots for OTA detection at different concentrations (A); Variations of R_{CT} values as a function of OTA concentrations added to the immunosensor (inset); OTA standard curve concerning R_{CT} values (B). Delta R_{CT} values correspond to the difference between the RCT before and after antibody immobilization.

calculated LOD was 0.15 ng mL^{-1}.

3.5. Selectivity

As non-specific interactions can interfere with the performance of a biosensor, selectivity was evaluated using Ochratoxin B (OTB). This toxin has a structure similar to OTA, differing only in the absence of the chlorine atom dihydroisocoumarin. Both mycotoxins (OTA and OTB) were present at 25 ng mL^{-1} and the experiments were performed in triplicate. The percent change in RCT parameters was calculated as shown in Fig. S2 (Supplementary Material). The electrochemical response of the biosensor is much greater for OTA assays, in which the analyte forms a complex with the corresponding antibody (anti-OTA). The ΔR_{CT} values obtained were 431 Ω for OTA and 41 Ω for OTB. These results demonstrate the high selectivity of the developed biosensor and its applicability in detecting OTA.

Although other biosensors have been reported to detect OTA in different types of matrices, many of them are based on more labor-intensive and expensive methods. In addition, many are not efficient for real samples or were not evaluated for selectivity. Table 2 summarizes the analytical performance of some of these biosensors and compares them with the device developed in this study.

3.6. Application of the immunosensor in coffee samples

Samples of arabica coffee were contaminated with known concentrations of OTA. Analysis of the OTA-free matrix was also performed to verify the matrix's influence in the detection assay. These samples were also quantified with a commercial ELISA Kit from Elabscience. The details of this detection and standard curve are described in the

Table 2
Comparison of the analytical performance of the label-free impedimetric immunosensor with other biosensors for OTA detection.

Assay technique/Materials used	Matrix	Linear range (ng.mL^{-1})	LOD (ng.mL^{-1})	Selectivity	Recovery (%)	Reference
EIS (MBs-protein G/DCA)	Instant coffee	1.3–153.8	0.32	Not reported	80–100	[35]
EIS (Au/4-CP/Ab)	Not reported	1.0–20	0.5	Not reported	–	[25]
DPV (SPCE/4-CP/OTA-Apt)<	Cocoa beans	2–10	0.07	OTB	82.1–85	[36]
DPV (BSA/anti-OTA/PdNPs/CF)	Coffee	0,5-20	0,096	BSA AF-B1 Triptofano	93.2–98.9	[37]
EIS (Au/MBA/pA-G/AntiOTA)	Cocoa beans	0.01–5	0.01	Not reported	102–113	[23]
(Carbon//rGO/AgNPs/Apt/BSA)	Weet-Bix cereal	2–16	0.7	Not reported	94–106.25	[26]
EIS (Au/Cys/Anti-OTA)	Coffee	0.5–100	0,15	OTB	90.5–96.6	This work

Supplementary Material (Table S1 and Fig. S3). Table S1 presents the rates of OTA in the coffee samples, with variations from 90.5 to 96.6%. These results demonstrate the viability of the impedimetric immunosensor for full-scale applications.

4. Conclusions

A label-free electrochemical immunosensor was successfully developed for the detection of OTA. The biosensors fabrication was fully optimized to improve their performance using EIS. The calibration curve provided a broad linear range from 0.5 to 100 ng mL^{-1}, which is within the limits of interest for international legislation, and a LOD of 0.15 ng mL^{-1}. Recovery assays on an OTA-fortified coffee sample demonstrated that the biosensor is highly recommended for real samples. Furthermore, because of the small volume of sample used, the short time required for analysis, and the possibility of miniaturization, this biosensors developed here represent a promising analytical tool for on-site applications. Finally, it is worth mention that the developed prototype is versatile and can be applied to detect other mycotoxins or contaminants in commercially interesting grains, requiring only the change of recognition molecule.

Credit author statement

Jairo Pinto de Oliveira: Conceptualization; Data curation; Formal analysis; Funding acquisition; Investigation; Methodology; Software; Validation; Visualization; Roles/Writing - original draft; Writing - review & editing. **Francisco Burgos-Flórez:** Data curation; Formal analysis; Investigation; Methodology; Writing - review & editing, **Isabella Sampaio:** Data curation; Formal analysis; Investigation; Methodology; Writing - review & editing. **Pedro Villalba:** Writing - review & editing. **Valtencir Zucolotto:** Conceptualization; Project administration; Resources; Writing - review & editing.

Declaration of competing interest

The authors declare that they have no known competing financial interests or personal relationships that could have appeared to influence the work reported in this paper.

Data availability

Data will be made available on request.

Acknowledgments

We gratefully acknowledge CNPq – Brazil (Grant numbers 150729/2021–9) and FAPES – Brazil (Grant numbers 436/2021) for the financial support and the researchers from Nanomedicine and Nanotoxicology Group for their cooperation in our studies. This research used facilities of the Brazilian Nanotechnology National Laboratory (LNNano), part of the Brazilian Center for Research in Energy and Materials (CNPEM), a private non-profit organization under the supervision of the Brazilian Ministry for Science, Technology, and Innovations (MCTI). The Microfabrication staff is acknowledged for the assistance during the experiments (Proposal 20220010).

Appendix A. Supplementary data

Supplementary data to this article can be found online at https://doi.org/10.1016/j.talanta.2023.124586.

References

[1] World Health Organization, Mycotoxins in African Foods: Implications to Food Safety and Health (AFRO Food Safety (FOS), 2006. Issue No. July 2006.
[2] FAO – Fundação das Naçoes Unidas para Alimentaçao e Agricultura. Disponível em http://www.fao.org/food/food-safety-quality/a-z-index/coffee/en/.
[3] I. Studer-Rohr, J. Schlatter, D.R. Dietrich, Kinetic parameters and intraindividual fluctuations of ochratoxin A plasma levels in humans, Arch. Toxicol. 74 (2000) 499–510, https://doi.org/10.1007/s002040000157.
[4] K. Hao, S. Suryoprabowo, S.S. Song, L.Q. Liu, H. Kuang, Food Agric. Immunol. 29 (2018) 498—510.
[5] P.A. Murphy, S. Hendrich, C. Landgren, C.M. Bryant, J. Food Sci. 71 (2006) R51—R65.
[6] E.E. Creppy, F.C. Størmer, D. Kern, R. Röschenthaler, G. Dirheimer, Effects of ochratoxin A metabolites on yeast phenylalanyl-tRNA synthetase and on the growth and in vivo protein synthesis of hepatoma cells, Chem. Biol. Interact. 47 (1983) 239–247, https://doi.org/10.1016/0009-2797(83)90160-6.
[7] H. Assaf, H. Azouri, M. Pallardy, Ochratoxin A induces apoptosis in human lymphocytes through down regulation of BCL-xl, Toxicol. Sci. 79 (2004) 335–344, https://doi.org/10.1093/toxsci/kfh123.
[8] G.A. Boorman, H.L. Hong, M.P. Dieter, H.T. Hayes, A.E. Pohland, M. Stack, M. I. Luster, Myelotoxicity and macrophage alteration in mice exposed to ochratoxin A, Toxicol. Appl. Pharmacol. 72 (1984) 304–312, https://doi.org/10.1016/0041-008X(84)90315-6.
[9] G. Müller, B. Burkert, H. Rosner, H. Köhler, Effects of the mycotoxin ochratoxin A and some of its metabolites on human kidney cell lines, Toxicol. Vitro 17 (2003) 441–448, https://doi.org/10.1016/S0887-2333(03)00053-5.
[10] F. Malir, V. Ostry, A. Pfohl-Leszkowicz, E. Novotna, A. Ochratoxin, Developmental and reproductive toxicity—an overview, Birth Defects Res. B Dev. Reprod. Toxicol. 98 (2013) 493–502, https://doi.org/10.1002/bdrb.21091.
[11] T. Lea, K. Steien, F. Størmer, Mechanism of ochratoxin A-induced immunosuppression, Mycopathologia 107 (1989) 153–159, https://doi.org/10.1007/BF00707553.
[12] V. Myndrul, R. Viter, M. Savchuk, N. Shpyrka, D. Erts, D. Jevdokimovs, V. Silamiķelis, V. Smyntyna, A. Ramanavicius, I. Iatsunskyi, Porous silicon based photoluminescence immunosensor for rapid and highly-sensitive detection of Ochratoxin A, Biosens. Bioelectron. 102 (2018) 661–667.
[13] R. Viter, M. Savchuk, I. Iatsunskyi, Z. Pietralik, N. Starodub, N. Shpyrka, A. Ramanaviciene, A. Ramanavicius, Analytical, thermodynamical and kinetic characteristics of photoluminescence immunosensor for the determination of Ochratoxin A, Biosens. Bioelectron. 99 (2018) 237–243.
[14] N. Adányi, I.A. Levkovets, S. Rodriguez-Gil, A. Ronald, M. Váradi, I. Szendrő, Development of immunosensor based on OWLS technique for determining Aflatoxin B1 and Ochratoxin A, Biosens. Bioelectron. 22 (2007) 797–802.
[15] S. Alarcon, G. Palleschı, D. Compagnone, M. Pascale, A. Vısconti, I. Barnavetro, Monoclonal antibody based electrochemical immunosensor for the determination of ochratoxin A in wheat, Talanta 69 (2006) 1031–1037.
[16] M. Muchindu, E. Iwuoha, E. Pool, N. West, N. Jahed, P. Baker, T. Waryo, A. Williams, Electrochemical ochratoxin A immunosensor system developed on sulfonated polyaniline, Electroanalysis 23 (2011) 122–128.
[17] M. Badea, L. Floroian, P. Restani, S.C.A. Cobzac, M. Moga, Ochratoxin A detection on antibody-immobilized on BSA-functionalized gold electrodes, PLoS One 11 (2016), e0160021.
[18] X.-P. Liu, Y.-J. Deng, X.-Y. Jin, L.-G. Chen, J.-H. Jiang, G.-L. Shen, R.-Q. Yu, Ultrasensitive electrochemical immunosensor for ochratoxin A using gold colloid-mediated hapten immobilization, Anal. Biochem. 389 (2009) 63–68.
[19] A. Karczmarczyk, A.J. Baeumner, K.-H. Feller, Rapid and sensitive inhibition-based assay for the electrochemical detection of Ochratoxin A and Aflatoxin M1 in red wine and milk, Electrochim. Acta 243 (2017) 82–89.
[20] Y. Wang, G. Ning, Y. Wu, S. Wu, B. Zeng, G. Liu, et al., Facile combination of beta-cyclodextrin host-guest recognition with exonuclease-assistant signal amplification for sensitive electrochemical assay of ochratoxin A, Biosens. Bioelectron. 124 (125) (2019) 82–88, https://doi.org/10.1016/j.bios.2018.10.007.
[21] M. Baccarin, F.A. Santos, F.C. Vicentini, B. Janegitz, V. Zucolotto, O. Fatibello, Electrochemical sensor based on reduced graphene oxide/carbon black/chitosan composite for the simultaneous determination of dopamine and paracetamol concentrations in urine samples, J. Electroanal. Chem. 799 (2017) 436–443.
[22] M.J. Schöning, A. Poghossian, Label-free Biosensing: Advanced Materials, Devices and Applications, Elsevier, 2018.
[23] F. Malvano, D. Albanese, R. Pilloton, M. Di Matteo, A highly sensitive impedimetric label free immunosensor for Ochratoxin measurement in cocoa beans, Food Chem. 212 (2016 Dec 1) 688–694, https://doi.org/10.1016/j.foodchem.2016.06.034. Epub 2016 Jun 14. PMID: 27374585.
[24] M. Muchindu, E. Iwuoha, E. Pool, N. West, N. Jahed, P. Baker, T. Waryo, A. Williams, Electrochemical ochratoxin A immunosensor system developed on sulfonated polyaniline, Electroanalysis 23 (2011) 122–128, https://doi.org/10.1002/elan.201000452.
[25] Abd-Elgawad Radi, Xavier Muñoz-Berbel, Vasilica Lates, Jean-Louis Marty, Label-free impedimetric immunosensor for sensitive detection of ochratoxin A, Biosens. Bioelectron. 24 (7) (2009) 1888–1892, https://doi.org/10.1016/j.bios.2008.09.021.
[26] Kwanele Kunene, Myalowenkosi Sabela, Suvardhan Kanchi, Mikhael Bechelany, Bisetty Krishna, Functionalized electrochemical aptasensor for sensing of ochratoxin A in cereals supported by in silico adsorption studies, ACS Food Science & Technology (2021), https://doi.org/10.1021/acsfoodscitech.1c0022.
[27] H. Akafzade, S.C. Sharma, N. Hozhabri, W. Chen, L. Ma, Raman spectroscopy analysis of new copper-cysteamine photosensitizer, J. Raman Spectrosc. 50 (2019) 522–527, https://doi.org/10.1002/jrs.5541Raman.
[28] J.R. Ferraro, K. Nakamoto, C.W. Brown, Introductory Raman Spectroscopy, second ed., Academic Press, Amsterdam; Boston, 2003 (Raman).

[29] A. Pawlukojc, I. Natkaniec, I. Majerz, L. Sobcyk, Spectrochim. Acta A, 2001, 57, 2775, in: A. Pizzi, K.L. Mittal (Eds.), Handbook of Adhesive Technology, Revised and Expanded, 2th Edition vol. 1036, CRC Press, 2003, 978-0824709860.
[30] S.W. Ellepola, S.-M. Choi, D.L. Phillips, C.-Y. Ma, Raman spectroscopic study of rice globulin, J. Cereal. Sci. 43 (1) (2006) 85–93, https://doi.org/10.1016/j.jcs.2005.06.006.Ref 39 do review.
[31] A. Pizzi, K.L. Mittal, Handbook of Adhesive Technology, Revised and Expanded (2, Ilustrado, Edição Revisada), CRC Press, 2003, p. 1036, 978-0824709860.
[32] V. Shunko Evgeny, V. Belkin Veniamin, Cleaning properties of atomic oxygen excited to metastable state 2s22p4(S10), J. Appl. Phys. 102 (8) (2007), 083304–1–14. Bibcode: 2007JAP 102h3304S.doi: 10.1063/1.2794857.
[33] Robert D. Deegan, Olgica Bakajin, Todd F. Dupont, Greg Huber, Sidney R. Nagel, Thomas A. Witten, Nature 389 (1997) 827–829, https://doi.org/10.1038/39827.
[34] Akhtar Hayat, Lise Barthelmebs, Jean-Louis Marty, Electrochemical impedimetric immunosensor for the detection of okadaic acid in mussel sample, Sensor. Actuator. B Chem. (2012) 810–815, https://doi.org/10.1016/j.snb.2012.05.075. Volumes 171–172.
[35] A. Jodra, M. Hervas, M.A. Lopez, A. Escarpa, Disposable electrochemical magneto immunosensor for simultaneous simplified calibration and determination of Ochratoxin a in coffee samples, Sens. Actuators, B 221 (2015) 777–783, https://doi.org/10.1016/j.snb.2015.07.007.
[36] Rupesh K. Mishra, Akhtar Hayat, Gaëlle Catanante, Georges Istamboulie, Jean-Louis Marty, Sensitive quantitation of Ochratoxin A in cocoa beans using differential pulse voltammetry based aptasensor, Food Chem. 192 (2016) 799–804, https://doi.org/10.1016/j.foodchem.2015.07.080.
[37] K. Kunene, M. Weber, M. Sabela, D. Voiry, S. Kanchi, K. Bisetty, M. Bechelany, Highly-efficient electrochemical label-free immunosensor for the detection of ochratoxin A in coffee samples, Sensor. Actuator. B Chem. (2019), 127438, https://doi.org/10.1016/j.snb.2019.127438.